An OGCM Simulation of Seasonal and Interannual Variabilities in the Surface-Layer Pacific of the Equatorial Band[1]

Boyin Huang[2] and Zhengyu Liu

Department of Atmospheric and Oceanic Sciences, University of Wisconsin-Madison 1225 W. Dayton St., Madison, WI-53706, U.S.A.

(Received June 18, 2001; revised October 26, 2001)

ABSTRACT

The heat budget is analyzed in the surface-layer (0-50 m) Pacific of the equatorial band (10°S-10°N), using the simulation of an ocean general circulation model from 1945 to 1993. The analysis indicates that downward net surface heat flux from the atmosphere and ocean advective heat fluxes play distinct roles in seasonal and interannual variabilities of surface-layer ocean temperature. The surface heat flux dominantly determines the ocean temperature in the seasonal time-scale. But, it has a negative feedback to the ocean temperature in the interannual time-scale. The interannual variability of ocean temperature is largely associated with the cold advection from off-equatorial divergent flow in the central Pacific and from upwelling in the cold tongue. Both the surface heat flux and ocean advective heat fluxes are important to the ocean temperature during an El Niño event. The ocean advective heat fluxes are further associated with local westward trade wind in the central Pacific. These results are largely consistent with some regional observational analyses.

Key words: Seasonal variability, Interannual variability, Heat flux

1. Introduction

The physical mechanisms controlling the El Niño event have been studied based on observations in the equatorial Pacific (Weare 1983; Reed 1986; Hayes et al. 1991; McPhaden and Picaut 1990; Frankignoul et al. 1996; Weisberg and Wang 1997). One of the most important issues is whether the surface heat flux or ocean advective heat fluxes are dominant in controlling the sea surface temperature (SST). Some studies indicated that the SST is mainly controlled by the surface heat flux from atmosphere, while other studies showed that ocean advective heat fluxes might be more important in influencing SST due to different diagnosis methods, data periods and locations. These studies suggest that the mechanisms in each El Niño event might be different, and more independent investigations are needed to further understand the fundamental characteristics of the El Niño.

An alternative method to study the El Niño is the numerical simulation based on ocean general circulation model (OGCM). The intercomparison between simulation and observation

[1] Corresponding author address: Dr. Boyin Huang, Department of Earth, Atmospheric, and Planetary Sciences, Massachusetts Institute of Technology, Room 54-1721, 77 Massachusetts Ave., Cambridge, MA-02139, U.S.A.

[2] E-mail:bhuang@wind.mit.edu

may further help us understand the role of ocean and atmosphere in SST, and may have a clue to answer the questions of our interest: What are the roles of surface heat flux and ocean advective heat flux in the interannual variability of SST? Do these heat fluxes have the same role in different regions of the equatorial Pacific? Our simulation indicates that their roles are distinctive at different time–scales and in different regions.

The paper is organized as follows: The model performance and method of ocean heat budget diagnosis are presented in section 2. The closed ocean heat budget is analyzed for the surface–layer Pacific of the equatorial band in the seasonal (section 3), interannual (section 4) variabilities, and in an El Niño event (section 5). Section 6 is the summary.

2. Model

The Geophysical Fluid Dynamics Laboratory Modular Ocean Model (MOM2 beta, Pacanowski 1996) is used to simulate the oceanic heat budget in the Pacific equatorial band. The model domain extends globally from 80°S to 60°N with a coarse horizontal resolution of $2^\circ \times 2^\circ$ but a realistic topography. The vertical resolution is 25 m above 400 m. The model ocean is driven by the wind stress and net surface heat flux from atmosphere. The wind stress is calculated using monthly wind velocities from the Comprehensive Ocean and Atmosphere Data Set (COADS, da Silva et al. 1994). The surface heat fluxes are calculated based on Gill (1982):

$$Q_{\text{net}} = S_0 + H_{\text{L}} + H_{\text{S}} + H_{\text{IR}} \ , \tag{1}$$

$$H_{\text{L}} = - L\rho_{\text{a}} c_{\text{L}} |V|(q_{\text{s}} - q_{\text{air}}) \ , \tag{2}$$

$$H_{\text{S}} = - c_p \rho_{\text{a}} c_{\text{S}} |V|(T_{\text{s}} - T_{\text{air}}) \ , \tag{3}$$

$$H_{\text{IR}} = - \varepsilon\sigma T_{\text{s}}^4 (0.39 - 0.05\sqrt{e})(1 - 0.6c^2) \ , \tag{4}$$

where S_0, H_{L}, H_{S}, H_{IR} and Q_{net} represent downward fluxes of solar radiation, latent heat, sensible heat, infrared radiation, and net heat, respectively. q_{s} is saturated humidity that is a function of SST. T_{s} is the model ocean temperature of the first–layer (12.5 m). V, e, q_{air}, and T_{air} are the wind velocity, vapor pressure, humidity, and temperature of surface air in COADS. c is COADS total cloudiness, L is the latent heat of vaporization, c_p is the specific heat at constant pressure. ρ_{a} is the air density that is set to a constant of 1.2 kg m^{-3}. c_{L} and c_{S} are set to 0.92×10^{-3} and 1.5×10^{-3}, respectively. ε is the emissivity that is set to 0.95, and σ is the Stefan's constant. The model sea surface salinity is restored to Levitus (1982) monthly climatology with a restoring time of 100 days. The model initial temperature and salinity are set to Levitus annual mean climatology. The model is spun up for 500 years using monthly COADS data of 1945. The model is then integrated for 49 years using monthly COADS data from 1945 to 1993.

The capability of our coarse resolution OGCM to simulate the large–scale oceanic features can be seen in the model climatological temperature and currents. Figure 1a shows the mean temperature difference between the model (1945–1993) and Levitus (1982) climatology in the Pacific equatorial band (10°S–10°N). The simulated temperature is about 1–2°C lower than Levitus climatology above 200 m, and about 1–3°C higher between 200 and 400 m. The error may primarily result from the higher vertical diffusivity (1×10^{-4} m^2 s^{-1}) in our OGCM, and is a well–known problem of many OGCMs. The error of zonal average temperature in the Pacific (120°E–80°W) is relatively smaller above 200 m in the tropics (10°S–15°N) and the North Pacific north of 15°N (Fig. 1b). In addition, the long–term trends of the ocean

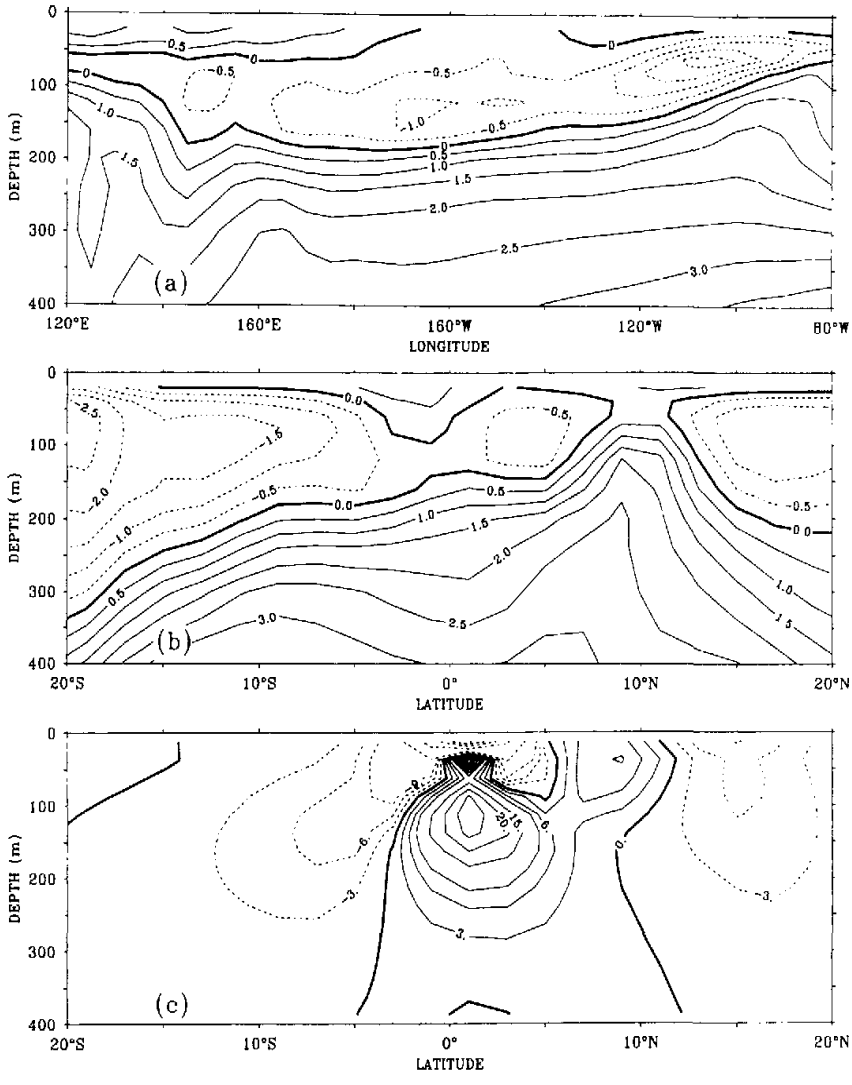

Fig. 1. (a) Mean temperature difference between simulation and Levitus averaged in the Pacific equatorial band (10°S–10°N). Contour interval is 0.5 K. (b) Same as (a) except averaged in the Pacific Ocean (120°E–80°W). (c) Simulated mean zonal currents averaged in the Pacific Ocean. Contour interval is 3 cm s^{-1} between −9 and 9, and 5 cm s^{-1} between −15 and −25.

temperature between 1955 and 1993 are also well simulated above 400 m in the tropical Pacific, the mid–latitude North Pacific, and the tropical Indian Ocean (Liu and Huang 2000; Huang and Liu 2001a and 2001b).

Our coarse resolution OGCM can also simulate the structure of the tropical currents reasonably (Fig. 1c), although the magnitude of currents is weaker than available observations (Wyrtki and Kilonsky 1984; Firing et al. 1998), eddy–resolving simulation (Semtner and

Chervin 1992), and the simulation of Philander et al. (1987) with higher resolution.

To understand the physical mechanisms of seasonal and interannual variabilities of the surface-layer (0–50 m) Pacific of the equatorial band, the closed heat budget is diagnosed using our coarse resolution OGCM in the warm pool, central Pacific, and cold tongue, respectively. We choose 10°S–10°N to represent the equatorial band of the Pacific. The equatorial band is further divided into 120°–170°E, 170°E–130°W, and 130°–80°W to represent the warm pool, central Pacific, and cold tongue. The closed heat budget can be written as

$$T_t = A_u + A_v + A_w + Q + q \ . \tag{5}$$

Here

$$T_t = \rho c_p H \overline{\hat{c}_x T} \ , \tag{6}$$

is spatially averaged ocean heat storage rate, and

$$(A_u, A_v, A_w) = \rho c_p H(-\overline{u\hat{c}_x T}, -\overline{v\hat{c}_y T}, -\overline{w\hat{c}_z T}) \ , \tag{7}$$

are spatially averaged ocean advective heat fluxes. H is the thickness of 50 m, and T is the model ocean temperature between 0 and 50 m. Q is downward net surface heat flux from the atmosphere, and q is upward turbulent heat flux from below 50 m:

$$q = -Q + \rho c_p H(\gamma \overline{\hat{c}_{zz} T} + \overline{F_{\text{turb}}}) \ , \tag{8}$$

where F_{turb} represents spatially averaged turbulent heat flux including mixing and convection, and γ is the vertical diffusivity. Other notations are conventional. The reason using advective form of heat flux instead of divergence form ($\nabla \cdot VT$) is to exclude the effect of mass flux in each spatial direction.

3. Seasonal variability

To resolve the seasonal variability properly, the model heat budget is diagnosed in the equatorial band of the Pacific every 10 days. The mean seasonal cycle is constructed by averaging 49 years simulation. Our analysis indicates that a semi-annual cycle is dominant in the warm pool and central Pacific, but an annual cycle is dominant in the cold tongue. The distribution of these semi-annual and annual cycles is consistent with the observation of Horel (1982).

In the warm pool (120°–170°E), the major feature is that the semi-annual cycle of surface heat flux (Q) largely determines the semi-annual cycle of ocean temperature (T, hereafter) averaged between 0 and 50 m. The semiannual cycle of Q and T is dominant (Fig. 2). Both Q and heat storage rate (T_t) reach their peaks in late April and late October, and they are the lowest in early February and early July with amplitude of about 20 and 15 W m^{-2}, respectively (Fig. 2a). Therefore, we conclude that Q is a predominant contributor to T in the warm pool as indicated in the observation of Fasullo and Webster (1999) and Lau and Sui (1997).

Another factor supporting our conclusion is that ocean advective heat fluxes have weak semi-annual cycle and small amplitude of variation. Therefore, they do not contribute very much to the semi-annual cycle of ocean temperature in the warm pool. On the contrary, the ocean advective heat fluxes exhibit an annual cycle, albeit very weak.

The features of seasonal cycle are very similar in the central Pacific between 170°E and 130°W (not shown) as in the warm pool. The semiannual cycle is dominant in Q and T_t.

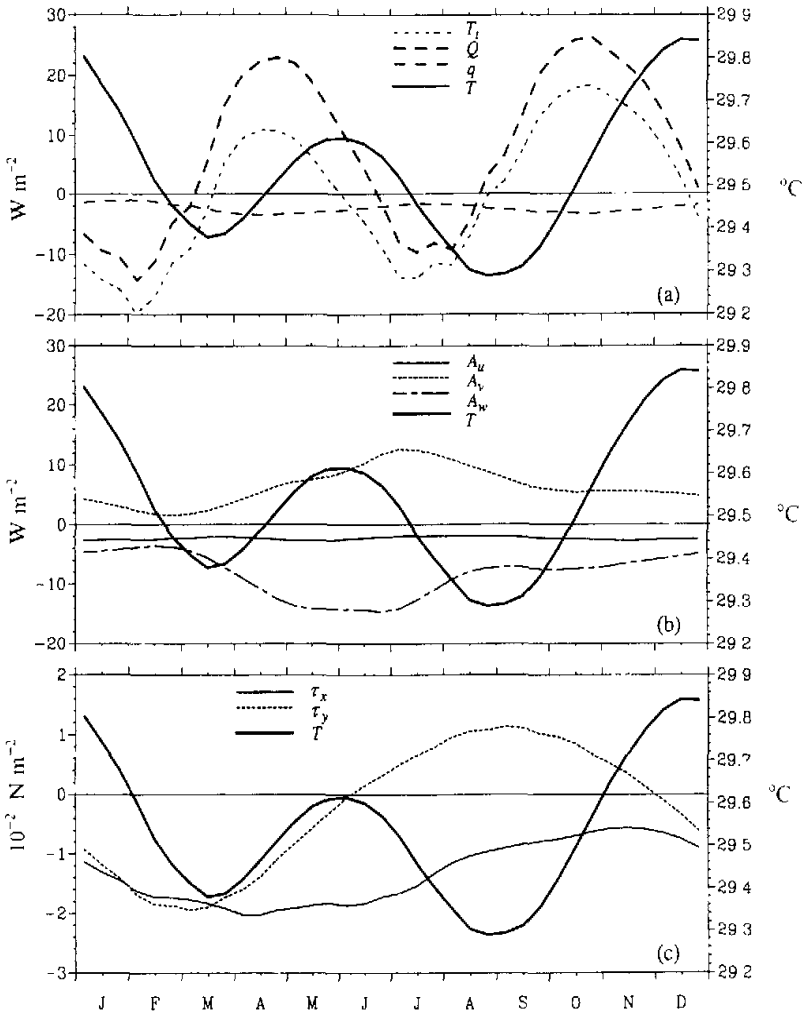

Fig. 2. Seasonal variabilities of ocean temperature (°C, right coordinate), ocean heat budget (W m^{-2}, left coordinate), and wind stress τ_x and τ_y (10^{-2} N m^{-2}, left coordinate) in the warm pool (120°–170°E)

but a weak annual cycle exhibits in ocean advective heat fluxes. Q is a major contributor to T. The main difference is that the heat flux due to off-equatorial divergent flow (A_v) is positive in the warm pool, but negative in the central Pacific.

In the cold tongue between 130°W and 80°W (Fig. 3a), however, the Q, T_t and T have a dominant annual cycle. T is largely associated with Q. But off-equatorial (A_v) and upwelling (A_w) advective heat fluxes also contribute to T. Q reaches its maximum in March and early July, its minimum in June–July with amplitude of about 45 W m^{-2}. The amplitude of T, is as

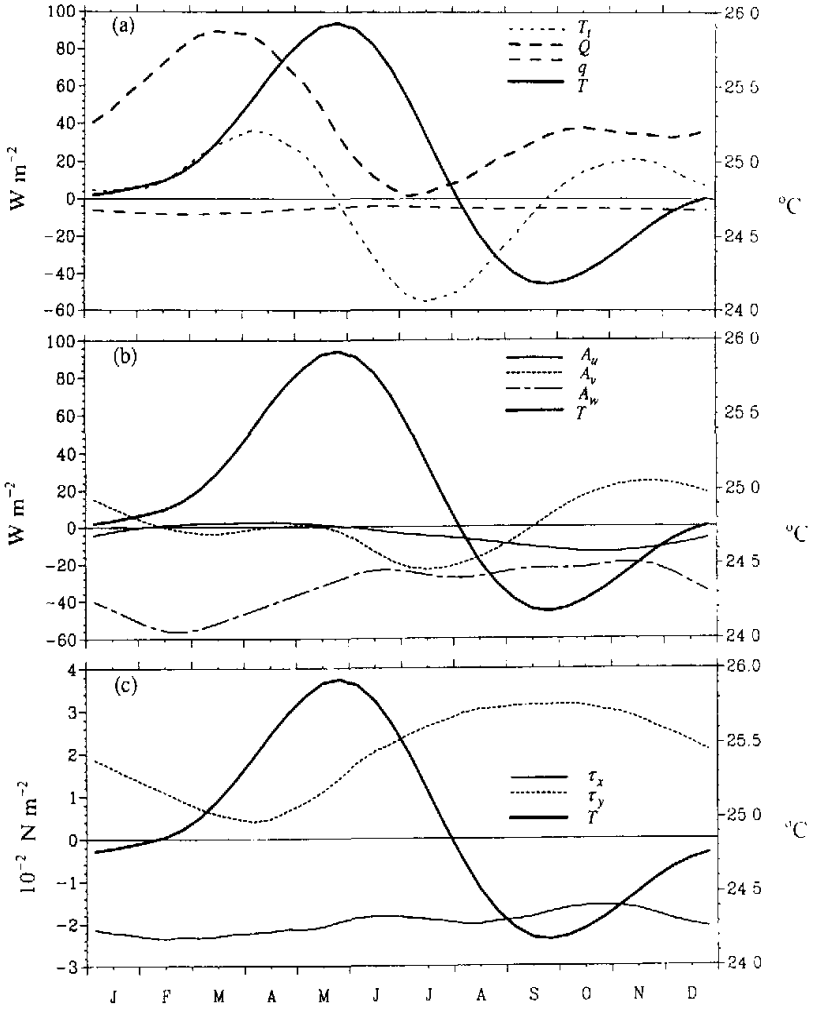

Fig. 3. Same as Fig. 2 except for the cold tongue (130°–80°W).

large as that of Q, such as in the warm pool. T_l lags Q about half month, but they are in phase in the warm pool. This suggests that the ocean advective heat fluxes have contributed to T_l in the cold tongue. Both the magnitude and amplitude of A_v and A_w are larger in the cold tongue (Fig. 3b) than in the warm pool, and are comparative with Q.

The characteristics of seasonal cycle of T_l in our simulation are consistent with observations (Wang and McPhaden 1999; Swenson and Hansen 1999) and other GCM simulations (Enfield 1986; Chen et al. 1994). But, we have to note that the magnitude of T_l is relatively smaller in our simulation due to coarse model resolution and average of a large area between 10°S and 10°N. In the warm pool, the westward cold advection (A_u) is very small and has no clear seasonal variability in our simulation (Fig. 2b). However, it is as large as the surface heat flux, and has a clear semiannual cycle in the observation of Tropical Atmosphere–Ocean

(TAO) in the mixed layer at 165°E at the equator (Wang and McPhaden 1999, their Figure 5d and Table 2). The seasonal cycle of A_u is also clear in the mixed layer between 5°S and 5°N in a simulation of 3-D reduced gravity primitive equation model (Chen et al. 1994, their Fig. 1a), although its magnitude is not as large as in Wang and McPhaden (1999). A_v is negative with maximum magnitude in May and June in our simulation but in October in Chen et al. (1994), while a positive A_v is observed during January and February in Wang and McPhaden (1999).

The observed A_v is a warm advection in the central Pacific at 170°W and 140°W at the equator in Wang and McPhaden (1999, their Figure 6c). But, it is a cold advection in the simulation within a mixed layer between 5°S and 5°N (Enfield 1986, his Fig. 8b) and in our study in the central Pacific. The simulated meridional cold advection in the central Pacific seems to be understandable: The westward trade wind forces the Ekman divergent flow, which transports relatively cooler water away from the equatorial ocean. The seasonal cycle of A_u in our simulation is very weak in comparison with Wang and McPhaden (1999), Enfield (1986), and Chen et al. (1994, their Fig. 1b). A reverse of the South Equatorial Current (SEC) from March to August is clearly observed in Chen et al. (1994) and Wang and McPhaden (1999), but no reverse is found in Enfield (1986) and our study.

The TAO observations in the cold tongue at 110°W at the equator indicate that the meridional advection in the cold tongue is a strong warm advection in all seasons (Wang and McPhaden 1999). But, it is a cold advection in the observation of a mixed layer between 5°S and 5°N from Swenson and Hansen (1999, their Fig. 5a with opposite sign), and simulation of Enfield (1986). Our simulation indicates that it is a warm advection from October to January, but a cold advection from June to August.

The major reason resulting in these differences might be: (1) coarse model resolution in our study, which results in weak ocean currents and therefore weak advective heat fluxes, (2) average of a large area in our study, which also results in a weak advective heat flux since ocean currents are weak away from the equator, and (3) a uniform depth of 50 m is used in our diagnosis, which reduces averaged vertical temperature gradient and upwelling current, and therefore reduces vertical advective heat flux in the cold tongue. It needs to be noted that the depth of mixed layer is diagnosed using a mixed layer model in Chen et al. (1994), and using a finite vertical temperature difference in Wang and McPhaden (1999) and Swenson and Hansen (1999). The mixed layer depth in Enfield (1986) is 50 m west of 145°W but 20 m east of 105°W.

4. Interannual variability

We calculated the annual mean ocean temperature and heat budget for each year from 1945 to 1993, using model output of every 10 days. The annual anomaly is calculated by subtracting the multi-year mean. Our simulation suggests that the surface heat flux is still an important factor contributing the ocean temperature. But, the interannual anomaly of surface-layer ocean temperature is largely associated with the ocean advection, which is different from the seasonal variability. The ocean advective heat fluxes are forced by local trade wind anomaly in the central Pacific.

First, the ocean temperature (T) averaged between 0 and 50 m does not seem to be associated with surface heat flux (Q) in the warm pool (120°-170°E), although the interannual anomaly of Q has an important impact on ocean heat storage rate (T_t). The correlation

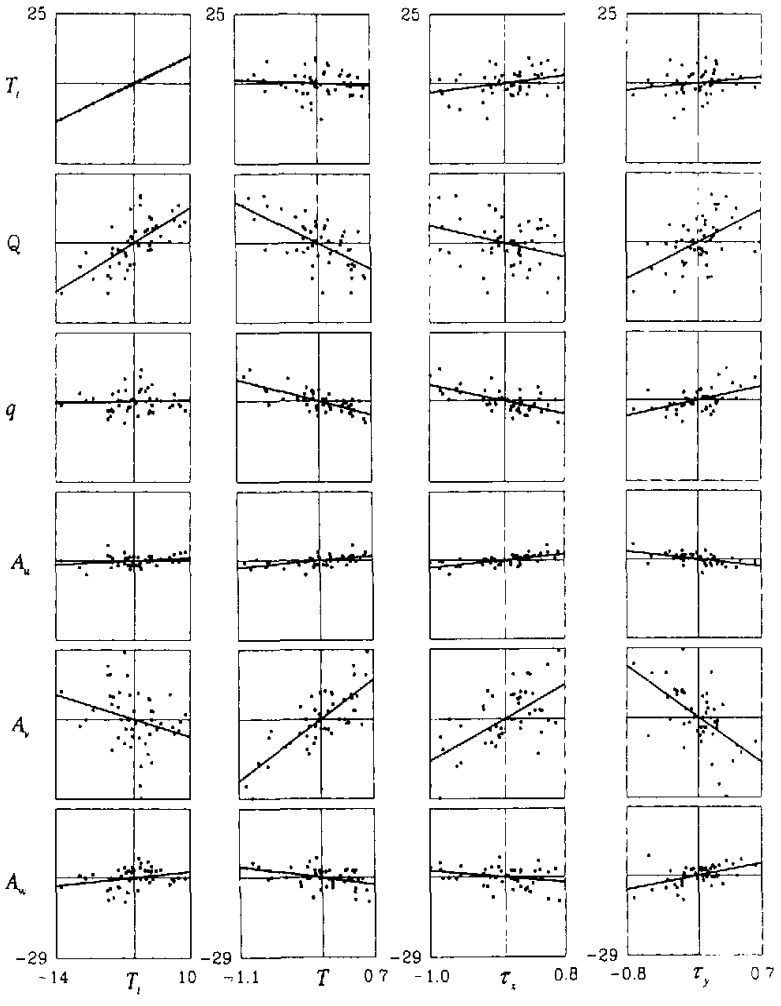

Fig. 4. Anomaly diagrams in the central Pacific (170°E–130°W). The y–coordinate represents the interannual heat budget anomalies T_t, Q, q, A_u, A_v, and A_w in W m^{-2} from the first to sixth row. The x–coordinate represents anomalies of heat storage rate T_t, temperature T (K), zonal wind stress τ_x (10^{-2} N m^{-2}), and meridional wind stress τ_y (10^{-2} N m^{-2}) from the 1st to 4th column. The solid lines represent the linear regression.

coefficient between T and Q is very small (Table 1). But the correlation coefficient between T_t and Q is 0.62. T is not directly associated with any ocean advective heat fluxes, although the anomalies of advective heat flux from upwelling (A_w) and off–equatorial divergent flow (A_v) are largely associated with southwestward trade winds in the warm pool.

In contrast, T is associated with both Q and A_v in the central Pacific (170°E–130°W). T_t is very well associated with Q (Fig. 4, the 1st column) as in the warm pool. Their correlation coefficient is 0.69 (Table 2). However, the T anomaly is negatively correlated (–0.63) with Q in the central Pacific (Fig. 4, the 2nd column), which suggests that Q acts as a negative

feedback to T. The T anomaly seems to be directly correlated (0.79) with A_v. An increase of T corresponds to a weakening A_v, and vise versa. A_v is further correlated (0.63) with the westward trade wind in the central Pacific. When the westward trade wind τ_x weakens, A_v weakens (both are positive anomaly) due to Coriolis effect, and vise versa (Fig. 4, the 3rd column). This weaker cold advection will in turn lead to a higher T.

Table 1. Correlation coefficient between the interannual anomalies of oceanic heat flux, T_t, T, τ_x, and τ_y in the Warm pool (120°–170°E). The bold coefficients indicate that its statistical significance is less than 95%.

	T_t	A_u	A_v	A_w	Q	q	T
T_t	1.00	**0.02**	**0.06**	**−0.02**	0.62	**0.03**	**−0.03**
T	**−0.03**	**−0.05**	**0.10**	**0.05**	**−0.17**	**−0.06**	1.00
τ_x	0.36	**−0.10**	−0.37	0.43	**0.17**	**−0.05**	**0.02**
τ_y	**−0.19**	−0.35	−0.47	0.54	**0.15**	**0.04**	**0.04**

Table 2. Same as Table 1 except for in the central Pacific (170°E–130°W)

	T_t	A_u	A_v	A_w	Q	q	T
T_t	1.00	0.26	−0.28	0.29	0.69	**0.05**	**−0.10**
T	**−0.10**	0.50	0.79	−0.42	−0.63	−0.73	1.00
τ_x	0.33	0.62	0.63	−0.30	−0.32	−0.63	0.74
τ_y	**0.19**	−0.51	−0.58	0.49	0.51	0.48	0.52

Slightly different from the central Pacific, T in the cold tongue (130°–80°W) is associated with both Q and A_w. The T_t is still correlated (0.54, Table 3) with Q as in the warm pool and central Pacific. Q has a negative feedback to T as in the central Pacific. T is positively correlated (0.50) with A_w in the cold tongue, but with A_v in the central Pacific. T increases when A_w weakens in the cold tongue, and vise versa. But, this upwelling does not seem to be associated with northwestward trade winds.

Table 3. Same as Table 1 except for in the cold tongue (130°–80°W)

	T_t	A_u	A_v	A_w	Q	q	T
T_t	1.00	**0.00**	**−0.04**	**0.08**	0.54	0.32	**−0.01**
T	**−0.01**	0.51	**−0.13**	0.50	−0.56	**−0.24**	1.00
τ_x	**−0.19**	0.34	**0.22**	**0.19**	−0.50	**−0.26**	**0.11**
τ_y	**0.21**	−0.42	**−0.10**	**0.07**	**0.22**	**0.12**	−0.33

In comparison with observations, our simulation shows that Q has a negative feedback to T, which is consistent with Wang and McPhaden (2000) and Weare (1983) in all three regions. However, the inconsistency between our simulation and observations is also significant. The correlation between T_t and Q is negative in the observations of Wang and McPhaden (2000), but positive in our simulation in all three regions (Tables 1–3). In their observations, T_t has a positive correlation with the cooling of A_w and westward advection (A_u) in all three regions. T_t has a positive correlation with A_v west of 170°W but negative to the east. In our simulation, it is true that T_t is positively correlated with A_u and A_w in

the central Pacific (Table 2). However, simulated T_t is negatively correlated with A_v in the central Pacific (Table 2), but not significantly correlated with ocean advective heat fluxes in the warm pool and cold tongue (Tables 1 and 3). The implication is that the effect of ocean advective heat fluxes is stronger in their observational study.

Again, the differences between the simulation and the observations may directly result from using a coarse resolution OGCM, the average of a large area, and different approximations in calculating the surface-layer ocean temperature. Other calculations should be very close. For example, Wang and McPhaden (2000) calculated the surface heat flux using observed SST, but we use the ocean temperature of 12.5 m in our simulation. They calculated I using a weekly averaged SST of Reynolds and Smith (1994). But, it is calculated based on each time step of one day in our simulation.

In addition, using monthly anomaly of ocean heat budget after filtering out the mean seasonal cycle, the cross-correlation study shows that T is positively correlated (0.40) with Q in the warm pool, when a phase lag of 12 months in T is considered. In the central Pacific and cold tongue, the corresponding correlation coefficient is 0.44 and 0.52, respectively, when a phase lag of 16, and 20 months in T is taken into account. This suggests that T could be affected by Q if a phase lag is considered.

5. Composite El Niño cycle

To address how the ocean temperature depends on surface heat flux and ocean advective heat fluxes in an El Niño event, the ensemble mean of ten major El Niño years is calculated to represent an "average" El Niño event. These ten El Niño years are 1948, 1953, 1958, 1963, 1965, 1969, 1973, 1979, 1983 and 1987, based on significantly higher SST in the eastern tropical Pacific Ocean (Horel 1982; Rasmusson and Carpenter 1982; Harrison and Larkin 1998). The variability regarding the El Niño is studied in an average period of four years, two years before and after the peak of an El Niño event. Our simulation shows that, similar to the interannual variability, the surface heat flux and ocean advective heat fluxes are important in an El Niño event in the central Pacific and cold tongue.

In the warm pool (120°–170°E), the ocean temperature (T) averaged between 0 and 50 m changes less than 0.1 K (Fig. 5), but it is slightly higher at year −1 (relative to the El Niño peak year 0). The amplitudes of surface heat flux (Q) and ocean advective heat fluxes are comparable, albeit small. The ocean heat storage rate (T_t) is very slight but positively correlated (0.49, Table 4) with Q. This suggests that Q may directly contribute to the change of T. On the other hand, T is negatively correlated (−0.49) with Q, which suggests that Q may have a negative feedback to T. The associations between the trade winds and Q (or ocean advective heat fluxes or T) are not clear in the warm pool.

Table 4. Correlation coefficient between oceanic heat flux, T_t, I, τ_x, and τ_y in an El Niño event in the warm pool (120°–170°E). The bold coefficients indicate that its statistical significance is less than 95%.

	T_t	A_u	A_v	A_w	Q	q	I
T_t	1.00	−0.48	0.23	**−0.00**	0.49	0.38	0.29
T	0.29	0.30	0.40	−0.32	−0.49	0.91	1.00
τ_x	0.18	−0.24	−0.46	0.54	**−0.08**	0.69	0.53
τ_y	−0.27	−0.51	−0.84	0.81	0.32	**−0.12**	**−0.05**

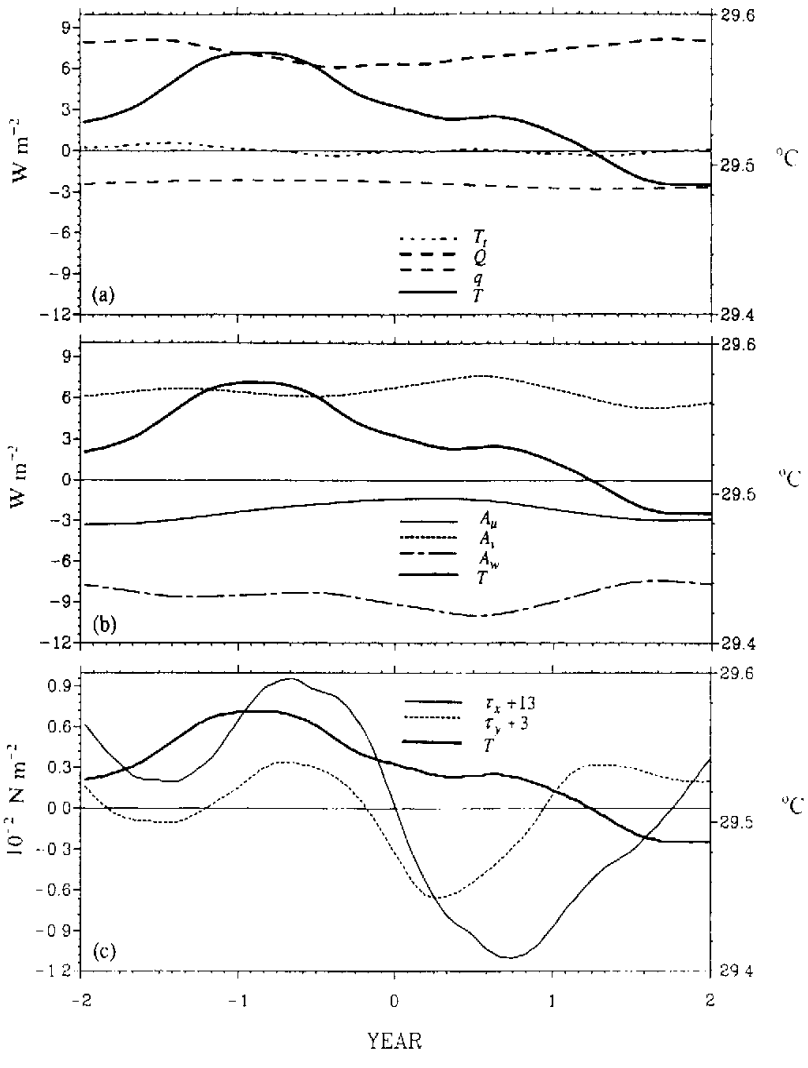

Fig. 5. Variabilities of ocean temperature (°C, right coordinate), ocean heat budget (W m^{-2}, left coordinate), and wind stress τ_x and τ_y (10^{-1} N m^{-2}, left coordinate) during the El Niño event in the warm pool (120°–170°E). The means of τ_x and τ_y are already subtracted and indicated in the legend.

In contrast, T in the central Pacific (170°E–130°W) is associated with Q and the ocean advective heat fluxes due to off-equatorial divergent flow (A_v) and upwelling (A_w). As shown in Fig. 6, T reaches its maximum in December of year −1, with amplitude of 0.7 K, which is much larger than that in the warm pool. Q reaches its minimum in April of year +1, and A_v reaches its minimum in February of year +1. Their amplitudes are comparable. T_t is very slight in the central Pacific as in the warm pool, but it is persistently positive during years

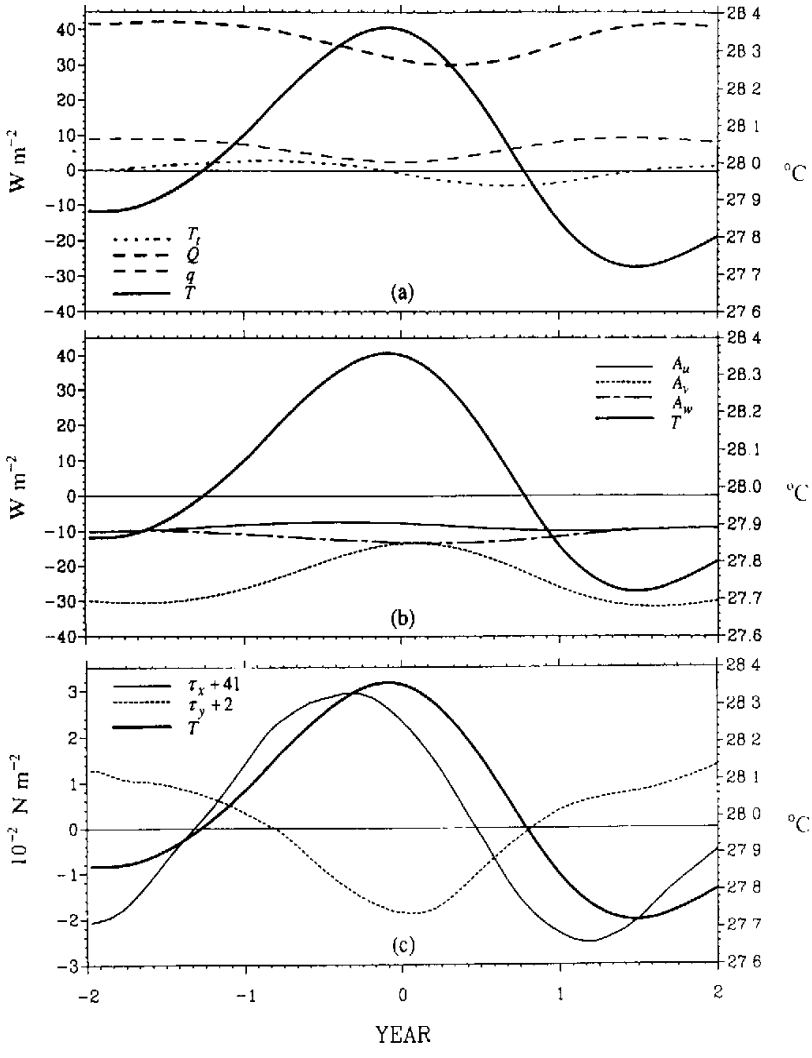

Fig. 6. Same as Fig. 5 except for the central Pacific (170°E–130°W).

−2 and −1, and negative during year 0 and from January to June of year +1. These positive and negative T_t well reflect the warming and cooling phases of an El Niño event (Fig. 6a). Further, T_t is well correlated (0.68, Table 5) with Q. The positive correlation between Q and T_t may be seen more clearly in their phase diagram (Fig. 7, the 1st column), which suggests that T could be associated with Q via T_t.

Table 5. Same as Table 4 except for in the central Pacific (170°E–130°W)

	T_t	A_u	A_v	A_w	Q	q	T
T_t	1.00	0.43	−0.33	0.48	0.68	**0.15**	**0.03**
T	**0.03**	0.84	0.92	−0.84	−0.69	−0.96	1.00
τ_x	0.44	0.98	0.70	−0.56	−0.35	−0.80	0.90
τ_y	0.28	−0.72	−0.99	0.94	0.88	0.98	−0.91

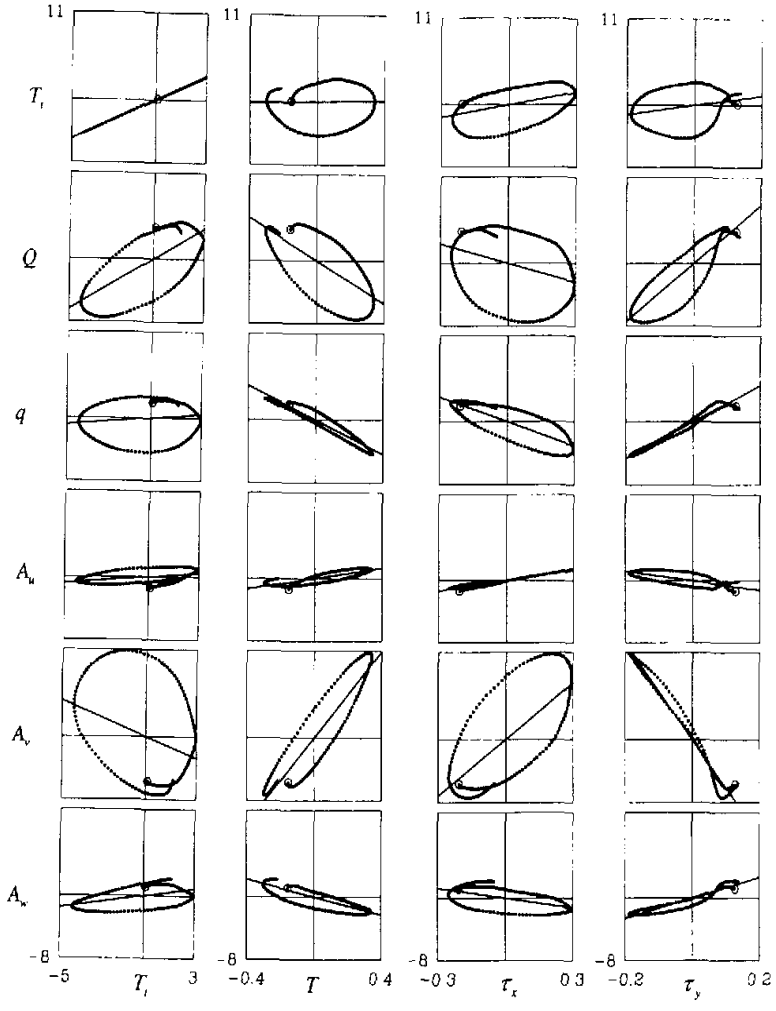

Fig. 7. Phase diagram in the central Pacific (170°E–130°W) during an El Niño event. The y-coordinate represents the heat budget anomalies T_t, Q, q, A_u, A_v, and A_w in W m^{-2} from the first to sixth row. The x-coordinate represents anomalies of heat storage rate T_t, temperature T (K), zonal wind stress τ_x (10^{-2} N m^{-2}), and meridional wind stress τ_y (10^{-2} N m^{-2}) from the 1st to 4th column. The larger circles indicate the starting point. The solid lines represent the linear regression.

On the other hand, T is negatively correlated (−0.69, Table 5) with Q, but positively correlated (0.92) with off-equatorial cold advection A_v (Figs. 6a, b, and the 2nd column of Fig. 7) in the central Pacific. This suggests a negative feedback between Q and T. T lags Q by approximately 9 months. T appears to be largely associated with A_v. But, we have to be cautious, since Q largely contributes to T_t. The implication is that both Q and ocean advective heat flux might be important to the change of T during an El Niño event in the

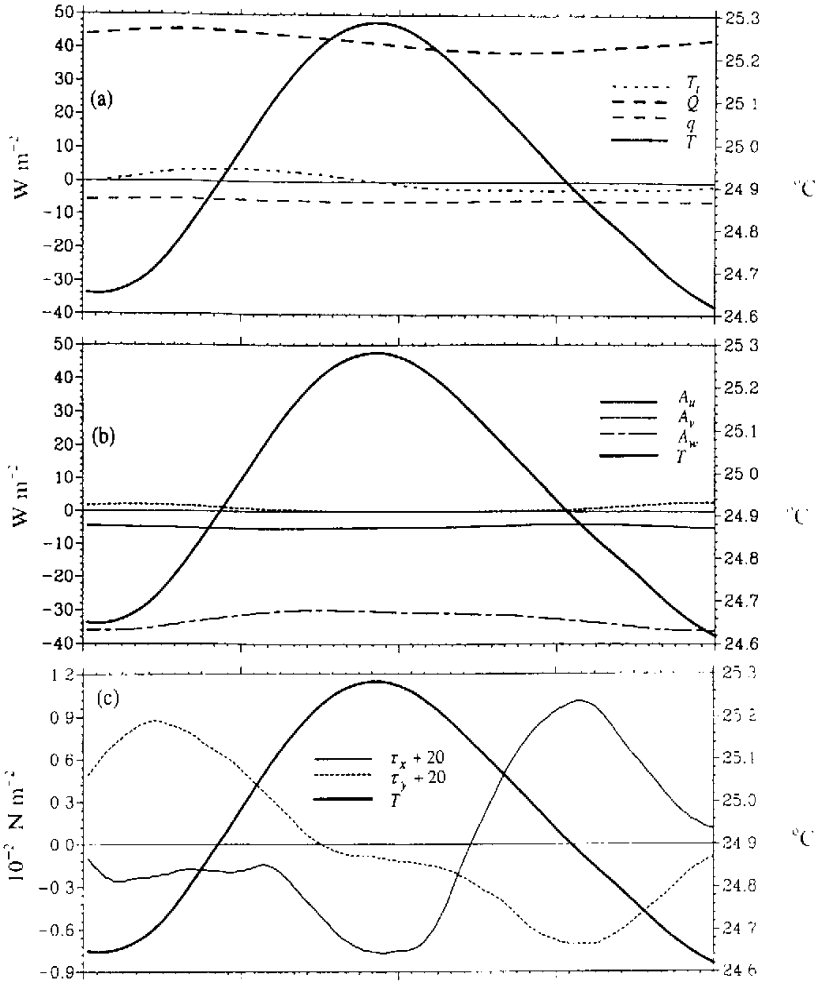

Fig. 8. Same as Fig. 5 except for the cold tongue (130°–80°W).

central Pacific.

Furthermore, A_v is strongly correlated (0.70, Table 5) with westward trade wind (Figs. 6b, c, and the 3rd column of Fig. 7) in the central Pacific. In the warming phase of an El Niño event, the westward trade wind decreases, which results in a weaker A_v due to less Ekman transport and a higher T. The correlation coefficient between the westward trade wind and T is very high (0.90).

As in the central Pacific, the evolution and correlation of Q, T_I, and T are very similar in the cold tongue between 130°W and 80°W (Fig. 8). The distinction is in the effect of ocean advective heat fluxes: The amplitude of Q is comparable with that of A_u in the cold tongue,

but with that of A_a in the central Pacific. The increase of T in an El Niño event is correlated (0.97, Table 6) with a weaker A_u in the cold tongue (Fig. 8b). However, A_u does not seem to be associated with northwestward trade winds (Figs. 8b and 8c).

Table 6. Same as Table 4 except for in the cold tongue (130°–80°W)

	T_t	A_a	A	A_u	Q	q	I
T	1.00	−0.76	**0.13**	0.17	0.90	0.38	**0.03**
T	**0.03**	−0.36	−0.94	0.97	−0.36	−0.74	1.00
τ_x	−0.54	0.82	0.23	−0.40	−0.45	0.42	0.48
τ_y	0.83	−0.61	0.37	−0.18	0.92	0.47	−0.24

Nevertheless, the effects of Q and ocean advective heat fluxes on El Niño events are very controversial. Some case studies indicated that surface net heat flux is more important than ocean advective heat fluxes (Weare 1983; Liu and Gautier 1990; Hayes et al. 1991; Weisberg and Wang 1997). Other case studies argued that ocean advective heat fluxes are more important (Reed 1986; McPhaden and Picaut 1990; Picaut and Delcroix 1995; Frankignoul et al. 1996). All these studies suggest that the mechanisms regarding each El Niño event may be different. Our conclusion regarding the importance of both surface heat flux and ocean advective heat fluxes is inferred from an "average" El Niño event.

In comparison with observations, the simulated warming in the warm pool region during the early stage of an El Niño event (December of year −2 and January −1) is consistent with Rasmusson and Carpenter (1982, their Fig. 17a), and Harrison and Larkin (1998). The correlation between westward trade wind and the cooling from westward cold advection seems to be consistent with Wyrtki's (1975) theory of warm water recharge and discharge during an El Niño event. However, the variation of westward cold advection is very small in our simulation. The correlation between westward trade wind and off-equatorial cold advection seems to be more significant in our simulation, owing to large amplitude of off-equatorial cold advection. Our simulation seems to show that an El Niño event in the cold tongue region is not directly driven by the decrease of trade winds, which is consistent with the observations of Rasmusson and Carpenter (1982, their Fig. 23), Harrison and Larkin (1998), and Wang (2000). Further studies including independent GCM simulations and observations are needed to validate our conclusions.

6. Summary

Using an OGCM simulation from 1945 to 1993, we have studied the seasonal and interannual variabilities of surface-layer ocean temperature (T) averaged between 0 and 50 m and the closed ocean heat budget in the equatorial band of the Pacific. Our conclusion is that the surface heat flux (Q) has a large contribution to T in the Pacific equatorial band between 10°S and 10°N at both seasonal and interannual time-scales. The ocean advective heat fluxes contribute greatly to the interannual variability of T in the central and eastern Pacific. These ocean advective heat fluxes may be associated with local trade winds.

The Q from the atmosphere has a dominant effect on T through ocean heat storage rate in the seasonal time-scale. The variability of ocean advective heat fluxes is smaller than that of Q, and has little effect on T. While in the interannual time-scale, Q has a negative feedback to T in the central Pacific and cold tongue, but not significant in the warm pool.

T in the central Pacific is largely associated with off-equatorial warm advection, which is further associated with westward trade wind. However, T in the cold tongue is associated with upwelling, although the upwelling is not significantly associated with the trade winds. During a typical El Niño event, both Q and ocean advective heat fluxes seem to have an important effect on T variability. Q has a negative feedback to T, and T lags the Q about nine months in the central Pacific. The off-equatorial divergent flow and upwelling contribute to T in the central Pacific and the cold tongue regions, respectively. The off-equatorial cold advection is associated with westward trade wind in the central Pacific. The effect of local trade winds and ocean advective heat flux on T seems to be relatively weak in the warm pool and cold tongue.

These phenomena in our OGCM are largely consistent with the available observations, although inconsistencies are not ignorable. The inconsistencies may partly be caused by our coarse resolution model, and the selection of the equatorial band between 10°S and 10°N. We have to note that our analysis represents only the ensemble estimate for the seasonal and interannual variabilities of ocean temperature and heat fluxes. Their mechanisms may be different for a specific season or year. In addition, the contribution of planetary waves may also be important (Battisti and Hirst 1989). Further investigation is expected.

It is interesting to note that the negative feedback between T and Q is also found in their long-term trends. The analysis of these trends (Liu and Huang 2000; Huang and Liu 2001a) indicated that downward net surface heat flux into the tropical Pacific Ocean has a negative feedback to the warming trend of surface-layer ocean between 0 and 50 m. They suggested that the long-term trend of surface-layer ocean temperature may be associated with wind-driven ocean currents, which provide an advective heat fluxes affecting the ocean temperature. Similar evidence is also found in the tropical Indian Ocean (Huang and Liu 2001b).

The distinction is, however, that T is probably associated with Q by a lagged response in the interannual time-scale. But, the lagged response in the long-term trends does not seem to be feasible. In addition, it is not clear whether the feedback between T and Q is positive or negative at the decadal time-scale. Further studies are needed.

We thank two anonymous reviewers whose comments have greatly improved our original manuscript.

REFERENCES

Battisti, D. S., and A. C. Hirst, 1989: Interannual variability in a tropical atmosphere-ocean model: Influence of the basic state, ocean geometry, and non-linearity. *J. Atmos. Sci.*, **46**, 1687-1712.

Chen, D., A. J. Busalacchi, and L. M. Rothstein, 1994: The role of vertical mixing, solar radiation, and wind stress in a model simulation of the sea surface temperature seasonal cycle in the tropical Pacific Ocean. *J. Geophys. Res.*, **99**, 20345-20359.

da Silva, A. M., C. C. Young, and S. Levitus, 1994: Atlas of Surface Marine Data 1994. NOAA Atlas NESDIS 6-8, U.S. Department of Commerce, NOAA, NESDIS, 912pp.

Enfield, D. B., 1986: Zonal and seasonal variations of the near-surface heat balance of the equatorial Pacific Ocean. *J. Phys. Oceanogr.*, **16**, 1038-1054.

Fasullo, J., and P. J. Webster, 1999: Warm pool SST variability in relation to the surface energy balance. *J. Climate*, **12**, 1292-1305.

Frankignoul, C., F. Bonjean, and G. Reverdin, 1996: Interannual variability of surface currents in the tropical Pacific during 1987-1993. *J. Geophys. Res.*, **101**, 3629-3647.

Firing, E., S. E. Wijffels, and P. Hacker, 1998: Equatorial subthermocline currents across the Pacific. *J. Geophys. Res.*, **103**, 21,413-21,423.

Gill, A. E., 1982: *Atmosphere-Ocean Dynamics*, Academic Press, Harcourt Brace Javanovich Publishers, 662pp.

Harrison, D. E., and N. K. Larkin, 1998: El Niño–southern oscillation sea surface temperature and wind anomalies, 1946–1993. *Rev. Geophysics*, **36**, 353–399.

Hayes, S. P., P. Chang, and M. J. McPhaden, 1991: Variability of the sea surface temperature in the eastern equatorial Pacific during 1986–88. *J. Geophys. Res.*, **96**, 10,553–10,566.

Horel, J. D., 1982: On the annual cycle of the tropical Pacific atmosphere and ocean. *Mon. Wea. Rev.*, **110**, 1863–1878.

Huang, B., and Z. Liu, 2001a: Temperature trend of the last 40 years in the upper Pacific Ocean. *J. Climate*, **15**, 3738–3750.

Huang, B., and Z. Liu, 2001b: Temperature trends in the upper tropical Indian Ocean: 1955–1993. *Dynamics of Atmospheric and Oceanic Circulations and Climate*, Edited by Institute of Atmospheric Physics, Chinese Academy of Sciences, Beijing, China, 413–433.

Lau, K. M., and C. H. Sui, 1997: Mechanisms of short-term sea surface temperature regulation: Observations during TOGA COARE. *J. Climate*, **10**, 465–472.

Levitus, S., 1982: *Climatological Atlas of the World Ocean*. NOAA Professional Paper 13, U.S. Department of Commerce, 173pp.

Liu, T. W., and C. Gautier, 1990: Thermal forcing on the tropical Pacific from satellite data. *J. Geophys. Res.*, **95**, 13,209–13,217.

Liu, Z., and B. Huang, 2000: Cause of the tropical Pacific warming. *Geophys. Res. Lett.*, **27**, 1935–1938.

McPhaden, M. J., and J. Picaut, 1990: El Niño–southern oscillation displacements of the western equatorial Pacific warm pool. *Science*, **250**, 1385–1388.

Pacanowski, R. C., 1996: *MOM2 Documentation*. GFDL Ocean Technical Report 3.2, 329pp.

Philander, S. G. H., W. J. Hurlin, and A. D. Seiged, 1987: Simulation of the seasonal cycle of the tropical Pacific Ocean. *J. Phys. Oceanogr.*, **17**, 1986–2002.

Picaut, J., and T. Delcroix, 1995: Equatorial wave sequence associated with warm pool displacements during 1986–1989 El Niño–La Niña. *J. Geophys. Res.*, **100**, 18,393–18,408.

Rasmusson, E. M., and T. H. Carpenter, 1982: Variations in the tropical sea surface temperature and surface wind fields associated with the Southern Oscillation / El Niño. *Mon. Wea. Rev.*, **110**, 354–384.

Reed, R. K., 1986: Effects of surface heat flux during the 1972 and 1982 El Niño episodes. *Nature*, **322**, 449–450.

Reynolds, R. W., and T. M. Smith, 1994: Improved global sea surface temperature analysis using optimum interpolation. *J. Climate*, **7**, 929–948.

Semtner, A. J., and R. M. Chervin, 1992: Ocean general circulation from a global eddy-resolving model. *J. Geophys. Res.*, **97**, 5493–5550.

Swenson, M. S., and D. V. Hansen, 1999: Tropical Pacific Ocean mixed layer heat budget: The Pacific cold tongue. *J. Phys. Oceanogr.*, **29**, 69–81.

Wang, C., 2000: The 1997–98 El Niño evolution relative to previous El Niño events. *J. Climate*, **13**, 488–501.

Wang, W., and M. J. McPhaden, 1999: The surface-layer heat balance in the equatorial Pacific Ocean. Part I: Mean seasonal cycle. *J. Phys. Oceanogr.*, **29**, 1812–1831.

Wang, W., and M. J. McPhaden, 2000: The surface-layer heat balance in the equatorial Pacific Ocean. Part II: Interannual variability. *J. Phys. Oceanogr.*, **30**, 2989–3008.

Weare, B. C., 1983: Interannual variation in net heating at the surface of the tropical Pacific Ocean. *J. Phys. Oceanogr.*, **13**, 873–885.

Weisberg, R. H., and C. Wang, 1997: Slow variability in the equatorial west-central Pacific in relation to ENSO. *J. Climate*, **10**, 1998–2017.

Wyrtki, K., 1975: El Niño—the dynamic response of the equatorial Pacific Ocean to atmospheric forcing. *J. Phys. Oceanogr.*, **5**, 572–584.

Wyrtki, K., and B. Kilonsky, 1984: Mean water and current structure during the Hawaii-Tahiti shuttle experiment. *J. Phys. Oceanogr.*, **14**, 242–254.